# Casimir-Lifshitz frictional heating in a system of parallel metallic plates

George V. Dedkov *

Posted Date: 13 September 2023

doi: 10.20944/preprints202309.0794.v1

Keywords: Casimir friction force, quantum friction force, radiative heating

*Article*

# Casimir-Lifshitz Frictional Heating in a System of Parallel Metallic Plates

**George V. Dedkov**

Kabardino-Balkarian State University, Chernysheskogo 174, Nalchik, 360004 Russia; gv_dedkov@e-mail.ru

**Abstract:** The Casimir–Lifshitz force of friction between neutral bodies in relative motion, along with the drag effect, causes their heating. This paper considers this frictional heating in a system of two metal plates within the framework of fluctuation electromagnetic theory. Analytical expressions for the friction force in the limiting cases of low (zero) temperature, low and high speeds, as well as general expressions describing the kinetics of heating, have been obtained. It is shown that the combination of low temperatures ($T < 10$ K) and velocities of $10 \div 10^3$ m/s provides most favourable conditions when measuring Casimir-Lifshitz friction force from heat measurements. In particular, the friction force of two coaxial discs of gold of 10 cm in diameter, one of which rotates at a frequency of $10 \div 10^3$ rps, can be measured using the heating effect by 1-2 K in less than 1 min. A possible experimental layout is discussed.

**Keywords:** Casimir-Lifshitz friction force; quantum friction; radiative heating

## 1. Introduction

Over the past two decades, much effort has been spent on investigating the static [1,2] and dynamic [3,4] Casimir effect in various geometric configurations, including a system of two parallel metal (dielectric) plates separated by a narrow vacuum gap. The main objective of these studies is the properties of a fluctuating electromagnetic field and its interaction with matter on the nanoscale. The measurement of these effects paves the way to the core of nonequilibrium quantum field theory [6–8].

In addition to the attractive (in most cases) Casimir forces between electrically neutral bodies at rest, a dissipative tangential force arises when one or both bodies move relative to each other. In this case, the corresponding fluctuation electromagnetic forces are called "van der Waals" [9], "Casimir" [10] or "quantum" [11] forces of friction. In our opinion, it is convenient to use the general name "Casimir-Lifshitz" (CL) friction force, which incorporates all the features of these dissipative forces regarding their distance, temperature and material properties.

It is worth noting that, despite many intense efforts, no convincing experimental measurements of the CL friction forces have been carried out to date. This is due not only to the small magnitude of these forces relative to the "ordinary" Casimir forces (forces of attraction), but also to the imperfections of the measurement layout. In particular, the effective interaction area and the relative velocity are significantly limited in the "pendulum" measurement scheme used in [12]. Other experimental scenarios [9,13–17] seem to be more exotic. Recently, in [15–17], in order to measure traces of quantum friction, the authors suggested a scenario, in which the nitrogen vacancy center in diamond acquires the geometric phase during rotation at a frequency of $10^3$–$10^4$ rps near the Si- or Au-coated surface. The nitrogen vacancy centers have been proposed for use as the main components of quantum computer processors [18].

Nearly all experiments to measure Casimir-Lifshitz forces (both conservative and dissipative) have been performed with well conducting materials (metals like gold) under near-normal temperature conditions. Regarding Casimir-Lifshitz friction forces, it has usually been assumed that they decrease with decreasing temperature, as the resistivity of metals and ohmic losses fall.

Preprints (www.preprints.org) | NOT PEER-REVIEWED | Posted: 13 September 2023 doi:10.20944/preprints202309.0794.v1



Therefore, at first glance, the friction force also does. The conclusion that for metals the temperature behavior of the CL friction is not so simple, was first made in [19] and later discussed in [20,21]. In has been shown that at temperatures $T \ll \theta_D$ ( $\theta_D$ is the Debye temperature) the force of friction can increase by several orders of magnitude compared to normal conditions. However, several issues have not been elucidated there, in particular, the relation between friction and heating effects at thermal nonequilibrium, relation between quantum friction and friction at close to zero temperature, kinetics of radiation heating, etc. The effects of thermal nonequilibrium on the CL forces and nonequilibrium thermodynamics of quantum friction have recently been considered in [22–25].

The main objective of this paper, in addition to studying CL friction and heating in a system of parallel metallic plates of nonmagnetic metals like gold, is to substantiate the possibility of determining the friction force from thermal measurements. In the calculations, the general results of fluctuation electrodynamics [26,27] are used, without a linear expansion in velocity in the basic expressions. It is shown that identical metal plates with different initial temperatures, moving with a constant nonrelativistic velocity $V$ relative to each other, rapidly reach the state of quasithermal equilibrium, continuing to heat up further. The heating rate is then determined by the power of the friction force.

The outline of this paper is as follows. In the next section, general relations between radiative heating and friction force for parallel plates in relative nonrelativistic motion are given. In Secs. 2.2–2.5, I consider the simplest case of identical plates of Drude metals having the same material parameters and temperature $T$. Analytical expressions are obtained for the friction force of metal plates in the limiting cases of low (zero) temperature, low and high speeds, as well as general expressions describing the kinetics of heating. In Sec. 3, the results of numerical calculations (heating rates of plate 1 and friction parameters $\eta = F_x/V$) are given for different thermal configurations and velocities. The analytical results of Sec. 2 are compared with the results of numerical integration according to the general formulas. Section 4 is devoted to a brief discussion of a possible layout of an experiment for determining the CL friction force by measuring the rates of heating of gold plates. Concluding remarks follow in Sec. 5. Appendixes A–C contain the details of analytical calculations. All formulas are written in the Gassian units, $\hbar, c$ are the Planck constant and the speed of light in vacuum, $T$ is the absolute temperature in units of the energy.

## 2. General Results

### *2.1. Radiative Heating and Friction Force for Parallel Plates in Relative Motion*

Here, we use the standard formulation of the problem, in which the plates are assumed to be made of homogeneous and isotropic materials with permittivities $\varepsilon_1$, $\varepsilon_2$ and permeabilities $\mu_1$, $\mu_2$, depending on the frequency $\omega$ and local temperatures $T_1$ and $T_2$ (Figure 1).

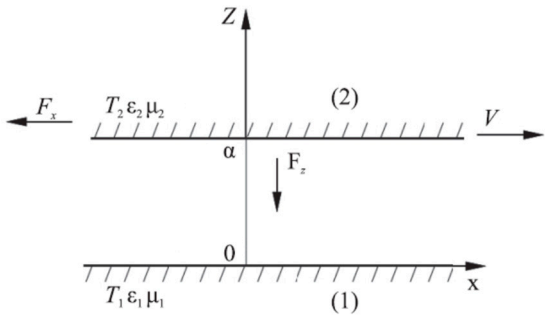


**Figure 1.** Configuration of parallel plates in relative motion.

In line with [26,27], the power $F_xV$ of the friction force $F_x$ per unit surface area applied to plate 2 in the laboratory coordinate system associated with plate 1, is given by

Preprints (www.preprints.org) | NOT PEER-REVIEWED | Posted: 13 September 2023 doi:10.20944/preprints202309.0794.v1



$$F_x V = P_1 + P_2/\gamma. \tag{1}$$

Here $P_1$ and $P_2$ are the heat fluxes of the plates from a unit surface area per unit time, and $\gamma = (1 - V^2/c^2)^{-1/2}$. For all quantities, indices 1 and 2 here and in what follows correspond to numbering in Figure 1. Moreover, $P_1$ and $P_2$ are calculated in the rest frames of the plates. General relativistic expressions for $P_1$ and $P_2$ were obtained in [26]. In the nonrelativistic case $V/c \ll 1$, but taking retardation into account, a more compact form of $P_1$ and $P_2$ reads [27]

$$P_1 = \frac{\hbar}{4\pi^3}\int_0^\infty d\omega\omega \int d^2k \frac{|q|^2}{|Q_m|^2}\mathrm{Im}\left(\frac{q_1}{\mu_1}\right)\mathrm{Im}\left(\frac{\tilde{q}_2}{\mu_2}\right)\left[\coth\left(\frac{\hbar\omega}{2T_1}\right) - \coth\left(\frac{\hbar\omega^-}{2T_2}\right)\right] + (\mu_{1,2} \leftrightarrow \varepsilon_{1,2}), \tag{2}$$

$$P_2 = -\frac{\hbar}{4\pi^3}\int_0^\infty d\omega \int d^2k\omega^- \frac{|q|^2}{|Q_m|^2}\mathrm{Im}\left(\frac{q_1}{\mu_1}\right)\mathrm{Im}\left(\frac{\tilde{q}_2}{\mu_2}\right)\left[\coth\left(\frac{\hbar\omega}{2T_1}\right) - \coth\left(\frac{\hbar\omega^-}{2T_2}\right)\right] + (\mu_{1,2} \leftrightarrow \varepsilon_{1,2}), \tag{3}$$

$$Q_m = (q + q_1/\mu_1)(q + \tilde{q}_2/\tilde{\mu}_2)\exp(qa) - (q - q_1/\mu_1)(q - \tilde{q}_2/\tilde{\mu}_2)(-qa). \tag{4}$$

Here $\omega^- = \omega - k_x V$, $q = \sqrt{k^2 - \omega^2/c^2}$, $q_{1,2} = \sqrt{k^2 - \varepsilon_{1,2}\mu_{1,2}\,\omega^2/c^2}$, and $a$ is the gap width in Figure 1. Variables with a tilde, such as $\tilde{q}_2$, should be used replacing $\omega \to \omega^-$ . The terms $(\mu_{1,2} \leftrightarrow \varepsilon_{1,2})$ are defined by the same expressions with appropriate replacements. In the general case, the expressions depending on $\varepsilon_{1,2}$ and $\mu_{1,2}$ correspond to the contributions of electromagnetic modes with P and S polarizations. The quantities $P_1$ and $P_2$ are directly related to the heating (cooling) rates of the plates: $dQ_1/dt = -P_1$ and $dQ_2/dt = -P_2$.

Using (1)–(4), the power of the friction force $F_x V = P_1 + P_2$ takes the form

$$F_x V = \frac{\hbar}{4\pi^3}\int_0^\infty d\omega \int d^2k(k_x V) \frac{|q|^2}{|Q_m|^2}\mathrm{Im}\left(\frac{q_1}{\mu_1}\right)\mathrm{Im}\left(\frac{\tilde{q}_2}{\mu_2}\right)\left[\coth\left(\frac{\hbar\omega}{2T_1}\right) - \coth\left(\frac{\hbar\omega^-}{2T_2}\right)\right] + (\mu_{1,2} \leftrightarrow \varepsilon_{1,2}). \tag{5}$$

Formula (5) can also be recast into a more familiar form in terms of the Fresnel reflection coefficients [9,23].

At $T_1 = T_2 = T$, due to the symmetry of the system, the heating rates of identical plates are equal. We then have $F_x V = 2P_{1,2}$, and the friction force can be determined using the heating rate of any plate. For $T_1 \neq T_2$, it follows $P_1 \neq P_2$, but $P_1(T_1, T_2) = P_2(T_2, T_1)$ and, correspondingly, $P_1(T_1, T_2) + P_2(T_1, T_2) = P_1(T_1, T_2) + P_1(T_2, T_1) = P_2(T_1, T_2) + P_2(T_2, T_1)$. This means that, when measuring the CL friction force, it is sufficient to control the temperature of only one plate.

### *2.2. Metal Plates in the Drude Model*

In order to treat the problem of temperature-dependent CL friction force between ordinary metals, we model them by the Drude model in terms of plasma frequency $\omega_p$ and damping parameter $\nu(T) = \omega_p^2\rho(T)/4\pi$, with $\rho(T)$ being the resistivity:

$$\varepsilon(\omega) = 1 - \frac{\omega_p^2}{\omega\left(\omega + \mathrm{i}\cdot\nu(T)\right)}. \tag{6}$$

Figure 2 plots the dependences $\rho(T)$ corresponding to the Bloch–Grüneisen (BG) model [28] and the modified Bloch–Grüneisen (MBG) model [29]. In the former case, the residual resistance is zero or can be specified by indicating the effective temperature, below which it is constant. In the MBG model, the residual resistivity is $\rho_0 = 2.3 \cdot 10^{-10}\Omega \cdot \mathrm{m}$ (see Figure 2).

Hereinafter, for simplicity, we assume that the plates are made of the similar nonmagnetic metal ($\mu_1 = \mu_2 = 1$) with the same plasma frequency $\omega_p$, but different dependence $\nu(T)$.

Preprints (www.preprints.org) | NOT PEER-REVIEWED | Posted: 13 September 2023 doi:10.20944/preprints202309.0794.v1



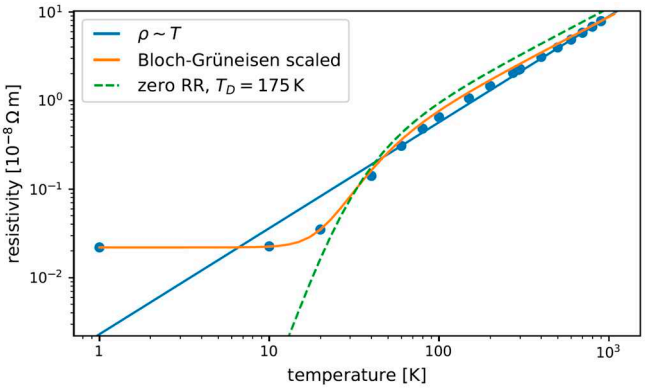


**Figure 2.** Resistivity of gold [26]. To obtain resistivity in the Gaussian units, one should use the relation $\Omega \cdot \mathrm{m} = (1/9)10^{-9}\mathrm{s}$.

Because $\varepsilon(\omega) \gg 1$ for good conductors, and the inequality gets stronger as $T \to 0$, the terms with $\varepsilon_{1,2}$ in (2) , (3), (5), corresponding to $P$ modes are negligible compared to the terms with $\mu_{1,2}$, corresponding to $S$ modes. So, in what follows, the contributions of *P* modes are omitted.

When calculating the integrals in (2), (3), (5), it is convenient to introduce a new frequency variable $\omega = \nu_m(T_1, T_2)t$ , with $\nu_m(T_1, T_2) = \max(\nu_1(T_1), \nu_2(T_2))$ and $\nu_i(T_i)$ being the damping parameters of plates 1 and 2 depending on their temperatures $T_1$ and $T_2$. The absolute value $k$ of the two-dimensional wave-vector (using the polar coordinates $k, \phi$ in the plane $(k_x, k_y)$) is expressed as $k = (\omega_p/c)\sqrt{y^2 + \beta_m^2 t^2}$ in the evanescent sector $k > \omega/c$ $(0 \le y < \infty)$ and $k = (\omega_p/c)\sqrt{\beta_m^2 t^2 - y^2}$ in the radiation sector $k < \omega/c$ $(0 \le y \le \beta_m t)$. Moreover, we introduce additional parameters $\beta_m = \nu_m/\omega_p$ , $\alpha_i = \hbar\nu_i/T_i$ , $\gamma_i = \nu_i/\nu_m$, $\lambda = \omega_p a/c$ , $\zeta = (V/c)\beta_m{}^{-1}$, and $K = \hbar\nu_m^2(\omega_p/c)^2/2\pi^3$. With these definitions, for $k > \omega/c$, Eqs. (2), (3) and (5) take the form

$$P_1 = K\int_0^\infty dt\int_0^\infty dy y^3 f_1(t,y), \tag{7}$$

$$P_2 = -K\int_0^\infty dt\int_0^\infty dy y^3 f_2(t,y), \tag{8}$$

$$F_x V = K\int_0^\infty dt\int_0^\infty dy y^3\sqrt{y^2+\beta_m^2 t^2} f_3(t,y), \tag{9}$$

$$f_1(t,y) = t\int_0^\pi d\phi\,\frac{\mathrm{Im}w_1\mathrm{Im}w_2}{|D|^2}Z(t,y,\phi), \tag{10}$$

$$f_2(t,y) = \int_0^\pi d\phi t^-\frac{\mathrm{Im}w_1\mathrm{Im}w_2}{|D|^2}Z(t,y,\phi), \tag{11}$$

$$f_3(t,y) = \zeta\int_0^\pi d\phi\cos\phi\,\frac{\mathrm{Im}w_1\mathrm{Im}w_2}{|D|^2}Z(t,y,\phi), \tag{12}$$

$$Z(t,y,\phi) = \coth\left(\frac{\alpha_1 t}{2}\right) - \coth\left(\frac{\alpha_2 t^-}{2}\right), \tag{13}$$

$$w_1 = \sqrt{y^2 + \frac{t}{t+\mathrm{i}\cdot\gamma_1}}\,, w_2 = \sqrt{y^2 + \frac{t^-}{t^-+\mathrm{i}\cdot\gamma_2}}\,, \quad t^- = t - \zeta\cos\phi\sqrt{y^2+\beta_m^2 t^2}, \tag{14}$$

Preprints (www.preprints.org) | NOT PEER-REVIEWED | Posted: 13 September 2023 doi:10.20944/preprints202309.0794.v1



$$D = (y + w_1)(y + w_2)\exp(\lambda y) - (y - w_1)(y - w_2)\exp(-\lambda y). \quad (15)$$

In the sector $k < \omega/c$, formulas (14), (15) should be modified by replacing $y \to iy$ and substituting $\beta_m t$ for $\infty$ in (7)–(9) in the integrals over $y$. The expressions for $\mathrm{Im}w_{1,2}$ can be additionally simplified. For example, it follows

$$\mathrm{Im}w_1 = \frac{\left(\sqrt{\{\gamma_1^2 y^2 + (1+y^2)t^2\}^2 + \gamma_1^2 t^2} - \gamma_1^2 y^2 - (1+y^2)t^2\right)^{1/2} \mathrm{sgn}(-t)}{\sqrt{2(\gamma_1^2 + t^2)}}. \quad (16)$$

The $\mathrm{Im}w_2$ is defined by the same expression (16), substituting $\gamma_2$ for $\gamma_1$ and $t^-$ for $t$. For two identical plates at quasithermal equilibrium, it follows $\gamma_1 = \gamma_2 = 1$, and a simpler useful expression is obtained by expanding the square root in (16) and leaving the expansion terms up to the second order:

$$\mathrm{Im}w_1 \approx \frac{|t| \cdot \mathrm{sgn}(-t)}{2\sqrt{(1+t^2)(y^2 + (1+y^2)t^2)}}. \quad (17)$$

In this case, an approximate analytical consideration can be carried out.

*2.3. Quantum Friction*

In the case $T_1 = T_2 = 0$, corresponding to the conditions of quantum friction, the main role is played by the evanescent modes $k > \omega/c$. At finite temperatures, the evanescent modes make the dominant contribution at $a < 1$ μm. This range of distances is very promising experimentally. For this reason, I consider hereinafter only evanescent modes, omitting the small term $\beta_m^2 t^2$ in (9), (14) and other formulas. So, at zero temperature, substituting the identity $Z(t, y, \phi) = \mathrm{sgn}(t) - \mathrm{sgn}\big(t - \zeta y \cos(\phi)\big)$ into Eq. (9) yields

$$F_x V = 2K\zeta \int_0^\infty dy y^4 \int_0^{\frac{\pi}{2}} d\phi \cos\phi \int_0^{\zeta y \cos\phi} dt \frac{\mathrm{Im}w_1 \mathrm{Im}w_2}{|D|^2}. \quad (18)$$

The simplest asymptotics of (18) can be worked out for two identical plates in the limit of low velocities, $\zeta \ll 1$. Using (15) and (17), we get

$$\mathrm{Im}w_1 \mathrm{Im}w_2 \to -\frac{t(\zeta y \cos\phi - t)}{4y^2}, |D|^2 \to \frac{1}{16} y^{-4} \exp(-2\lambda y). \quad (19)$$

Inserting (19) into (18) yields

$$F_x V = -\frac{\pi K}{2^{12}} \frac{\zeta^4}{\lambda^2} = -\frac{\hbar {\omega_p}^2}{2^{13}\pi^2} \left(\frac{\omega_p}{c}\right)^2 \left(\frac{V}{c}\right)^2 \left(\frac{V}{a\nu_0}\right)^2 = -\frac{1}{2^9} \frac{\hbar}{{\rho_0}^2 a^2} \left(\frac{V}{c}\right)^4, \quad (20)$$

where $\rho_0$ is the residual resistivity corresponding to the zero-temperature damping factor $\nu_0 = \nu(0)$.

The limit of large velocities, $\zeta \gg 1$ is more laborious. A reasonable representation of the triple integral in (9) can be worked out using an approximate expression for $\mathrm{Im}w_1 \mathrm{Im}w_2$, based on (17):

$$\mathrm{Im}w_1 \mathrm{Im}w_2 = \frac{|t(b-t)| \mathrm{sgn}(t) \mathrm{sgn}(b-t)}{4[(1+t^2)(1+(t-b)^2)(y^2 + t^2(1+y^2))(y^2 + (t-b)^2(1+y^2))]^{1/2}} \quad (21)$$

where $b = \zeta y \cos\phi$. The product $\mathrm{Im}w_1 \mathrm{Im}w_2$, as a function of $t$ in the range $0 \le t \le b$, reaches its maximum close to the point $t = b/2$, with zeroing at the end points $t = 0, t = b$ of the integration domain of the inner integral in (9). At the same time, the dependence on $t$ in $|D|^2$ is much weaker. By virtue of this, we insert $t = b/2$ into the denominator of (21) and into $|D|^2$(in the latter case, we also put $\cos\phi \approx 1$). Expression (21) then takes the form

$$\mathrm{Im}w_1 \mathrm{Im}w_2 \approx -\frac{t(b-t)}{4[(1+b^2/4)(y^2 + b^2(1+y^2)/4)]}. \quad (22)$$

With these transformations, it follows (see Appendix A)

Preprints (www.preprints.org) | NOT PEER-REVIEWED | Posted: 13 September 2023 doi:10.20944/preprints202309.0794.v1



$$F_x V = -\frac{K\zeta}{2}\int_0^\infty dy \frac{y^4}{|D|^2}\int_0^{\pi/2} d\phi \frac{\cos\phi}{\psi(y,\phi)}\int_0^{\zeta y\cos\phi} dtt(\zeta y\cos\phi - t), \tag{23}$$

where $|D|^2$ and $\psi(y,\phi)$ are given by (A2) and (A3). The integrals over $t$ and $\phi$ are calculated explicitly, and finally we get (see (A4) and (A6))

$$F_x V = -\frac{\hbar {v_0}^2}{3\pi^2}\left(\frac{\omega_p}{c}\right)^2\int_0^\infty dy \frac{y^5\exp(-2\lambda y)}{\left(y+\sqrt{1+y^2}\right)^4}\left(\frac{1}{y^2(1+y^2)} - \frac{2}{y^2\sqrt{y^2\zeta^2+4}} + \frac{2}{(1+y^2)\sqrt{(1+y^2)\zeta^2+4}}\right) \tag{24}$$

As follows from (24), in this approximation, the power of the friction force does not depend on the velocity at $\zeta \gg 1$. However, for $\zeta \ll 1$, this formula also agrees rather well with numerical calculations and approximation (20) (see Sec. 3.2).

*2.4. Low Temperatures, Linear in Velocity Approximation*

In the quasiequilibrium thermal regime, $T_1 = T_1 = T$, for two identical metal plates in the linear in velocity approximation, Eqs. (5) and (9) can be recast into the form [19,20]

$$F_x V = -\frac{\hbar V^2}{8\pi^2}\left(\frac{\omega_p}{c}\right)^4 \alpha^{-1} Y_1(\lambda,\alpha) \tag{25}$$

$$Y_1(\lambda,\alpha) = \alpha^2\int_0^\infty \frac{dt}{\sinh^2(\alpha t/2)}\int_0^\infty dy y^5 \frac{(\mathrm{Im} w_1)^2}{|D|^2}. \tag{26}$$

In this limit, the friction parameter $\eta = F_x/V$ does not depend on $V$. It is the dependence $F_x \propto \alpha^{-1}$ in (25) that leads to a large enhancement of friction at low temperatures, when $\alpha = \hbar\nu(T)/T \to 0$, because the function $Y_1(\lambda,\alpha)$ weakly depends on $\alpha$. The main contribution to $Y_1(\lambda,\alpha)$ in this case make the values $t < 1$, $y \sim 1/2\lambda \sim 1$, and we can again use (17) for $\mathrm{Im} w_1$. At the same time, $\alpha^2\sinh^{-2}(\alpha t/2) \approx 4/t^2$ (this is a good approximation at $\alpha < 0.3$) and $|D|^2 \approx 16y^4\exp(2\lambda y)$. Making use of these simplifications in (26), we arrive at (see Appendix B)

$$Y_1(\lambda,\alpha)) \approx \chi(\lambda) = \frac{\pi}{32}\left\{\frac{\pi}{4\lambda}[\mathrm{H}_1(2\lambda) - N_1(2\lambda)] - \frac{1}{4\lambda^2}\right\}, \tag{27}$$

where $\mathrm{H}_1(x)$ and $N_1(x)$ are the Struve and Neumann functions [30]. Using their series representations yields

$$\chi(\lambda) = \begin{cases} \frac{\pi}{64}\left(\frac{1}{\lambda} - \frac{1}{2\lambda^2} + \frac{1}{4\lambda^3} + \cdots\right), & \lambda \gg 1 \\ \frac{\pi}{32}\left(\frac{1}{4} + \frac{2\lambda}{3} - 2\lambda(\ln\lambda + 0.577)\right), & \lambda \ll 1 \end{cases} \tag{28}$$

An even simpler and physically clearer low-temperature representation of (25) is obtained by using the relation $\nu(T) = \omega_p^2\rho(T)/4\pi$ between the damping factor and resistivity, yielding

$$F_x V = -\frac{1}{2\pi}\left(\frac{V}{c}\right)^2\left(\frac{\omega_p}{c}\right)^2\frac{T}{\rho(T)}\chi(\lambda). \tag{29}$$

Combining the relation $\alpha \ll 1$, which implies $\hbar\nu(T) \ll T$, and $\zeta \ll 1$, which implies the limit of low-velocities $V/c \ll \nu(T)/\omega_p$, we conclude that formula (29) holds at

$$\omega_p V/c \ll \nu(T) \ll T/\hbar. \tag{30}$$

As a result, the conditions of low-temperature increase in friction and the applicability of the low-speed approximation are met at $V/c \ll T/\omega_p\hbar$. For gold, at $T = 1\,K$, this implies $V/c \ll 1.5\cdot 10^{-5}$.

Preprints (www.preprints.org) | NOT PEER-REVIEWED | Posted: 13 September 2023 doi:10.20944/preprints202309.0794.v1



According to [19,20], dependence (29) is associated with a growing penetration depth of S-polarized electromagnetic modes and an increase in their density at low temperatures. A significant low-temperature increase in the friction parameter was also noted in the case of movement of a metal particle above the metal surface [21].

*2.5. Low Temperatures, Large-Velocity Limit*

The limit $\zeta \gg 1$ at finite but low temperatures ($\alpha \ll 1$) can be analyzed similarly to the case of zero temperatures using the properties of function (21). When substituting (21) into (9) with allowance for (13), the first exponential term in (13) makes the dominant contribution at $t \sim 1 \ll b = \zeta y \cos\phi$. Because of this, we can take advantage of the substitution $|t-b| \to b$ in the denominator of (21). For the second term in (13), we introduce a new variable $t' = t - b$, and make the substitution $|t'+b| \to b$ in the denominator of (21), while the integral (9) is then determined by the large exponential factor $(\exp(\alpha t') - 1)^{-1}$ at $t' \sim 1 \ll b$. Then, taking into account these transformations in (9), and summing both contributions, the triple integral in (9) finally takes the form (see Appendix C)

$$I \approx \frac{\zeta^2}{2} \int_0^\infty dy y^4 |D|^{-2} \int_0^{\frac{\pi}{2}} d\phi\, \psi_1(y,\phi) \int_0^\infty dt \frac{t}{(e^{\alpha t} - 1)} \psi_2(y,\phi), \tag{31}$$

where

$$|D|^{-2} \approx \left(y + \sqrt{1+y^2}\right)^{-4} \exp(-2\lambda y), \tag{32}$$

$$\psi_1(y,\phi) = \cos^2\phi (1 + \zeta^2 y^2 \cos^2\phi)^{-1/2} (1 + \zeta^2 (1+y^2) \cos^2\phi)^{-1/2} \tag{33}$$

and

$$\psi_2(y,t) = \frac{1}{[(1+t^2)(y^2 + t^2(1+y^2)]^{1/2}} \tag{34}$$

To proceed further, we replace the function $t/(e^{\alpha t} - 1)$ by $1/\alpha$ in the inner integral (31), which is again a good approximation for $\alpha < 0.3$. The remaining integral yields

$$\int_0^\infty dt \frac{t}{(e^{\alpha t} - 1)} \psi_2(y,t) \approx \frac{1}{\alpha} \frac{\mathrm{K}(q)}{\sqrt{1+y^2}}, q = (1+y^2)^{-1/2}, \tag{34}$$

where $\mathrm{K}(q)$ is the complete elliptic integral [24]. Taking this into account, the $\phi$-integral in (31) can be evaluated as the arithmetic mean between the integrals calculated with the limit functions on the left and right sides of the inequality (see Appendix C)

$$\cos^2\phi (1 + \zeta^2 (1+y^2) \cos^2\phi)^{-1} < \psi_1(y,\phi) < \cos^2\phi (1 + \zeta^2 y^2 \cos^2\phi)^{-1}. \tag{35}$$

Substituting (C9) into (31) and (9) finally yields

$$F_x V = -\frac{T}{8\pi^2} V \left(\frac{\omega_p}{c}\right)^3 Y_2(\lambda,\zeta) \tag{36}$$

where $Y_2(\lambda,\zeta)$ is given by

$$Y_2(\lambda,\zeta) = \int_0^\infty dy \frac{y^4 e^{-2\lambda y}}{\left(y + \sqrt{y^2+1}\right)^4 (1+y^2)^{1/2}} \mathrm{K}\left(\frac{1}{\sqrt{1+y^2}}\right) \left[\frac{\sqrt{1+\zeta^2 y^2} - 1}{y^2 \sqrt{1+\zeta^2 y^2}} + \frac{\sqrt{1+\zeta^2(1+y^2)} - 1}{(1+y^2)\sqrt{1+\zeta^2(1+y^2)}}\right] \tag{37}$$

*2.6. Kinetics of Heating of Plates*

The heat transfer of plates is described by the equations

Preprints (www.preprints.org) | NOT PEER-REVIEWED | Posted: 13 September 2023 doi:10.20944/preprints202309.0794.v1



$$P_1(T_1,T_2)\Delta t = -h_1\rho_1 c_1(T_1)\Delta T_1,\ P_2(T_1,T_2)\Delta t = -h_2\rho_2 c_2(T_2)\Delta T_2, \tag{38}$$

with $c_i(T_i)$ being the specific heat capacities, $h_i$ and $\rho_i$ are the thicknesses and densities of materials, $P_1(T_1,T_2)$ and $P_2(T_1,T_2)$ are defined by Eqs. (2) and (3), and the temperature gains $\Delta T_i$ correspond to the interval of time $\Delta t$. The dependences $T_2(T_1)$ and $T_1(T_2)$ can be determined from the equation

$$\frac{dT_2}{dT_1} = \frac{P_1(T_1,T_2)c_1(T_1)h_1\rho_1}{P_2(T_1,T_2)c_2(T_2)h_2\rho_2}. \tag{39}$$

For identical plates, in (39), one can use the replacements $P_2(T_1,T_2) \to P_1(T_2,T_1)$, $P_1(T_1,T_2) \to P_2(T_2,T_1)$. Further on, we will consider only this case.

When writing Eqs. (38), (39), it is also assumed that the heat exchange due to radiative heat transfer occurs much slower than under thermal diffusion, and the plates acquire equal temperature at all points because of high thermal conductivity. Really, using the thermal diffusion equation along the normal to the plates, $\partial T/\partial t = a^2\,\partial^2 T/\partial z^2$, the characteristic time of the heat diffusion necessary to reach thermal quasiequilibrium, is $\tau = h^2/a^2$(where $a^2 = \kappa/c\rho$, and $\kappa$ is the thermal conductivity). Then it follows $\tau = h^2 c\rho/\kappa$ and in the case of gold at $T = 10$ K and $h_{1,2} = h = 500$ μ$m$ $c = 2.2$ J/(kg·K), $\kappa = 3200$ W/(m·K), $\rho = 19.8\cdot 10^3$kg/m$^3$ [31]) we obtain $\tau \simeq 3$ μs. In turn, the kinetics of heating induced by friction takes dozens of seconds or minutes (see Sec. 3.3), depending on the velocity and other parameters. Assuming that $P_i(T,T) = -0.5\eta(T,V)V^2$, from Eq. (38) we obtain

$$t = \frac{2h\rho}{V^2}\int_{T_0}^{T}\frac{c(T)}{\eta(T,V)}dT, \tag{40}$$

where $t$ is the heating time from the initial temperature $T_0$ to the final temperature $T$. In the simplest case $\eta = \text{const}$ and $c(T) = a_1T + a_2T^3$ (this is a typical low-temperature dependence for metals) it follows from Eq. (40) that

$$T(t) = \left(-\beta + \sqrt{\beta^2 + T_0^4 + 2\beta T_0^2 + 2\eta V^2 t/h\rho a_2}\right)^{1/2}, \tag{41}$$

where $\beta = a_1/a_2$. At $T_1 \neq T_2$ and relatively low velocities of plate 2, as follows from numerical calculations (see Sec. 3.1), the heating/cooling rates of metal plates differ only in sign, i.e. $P_1(T_1,T_2) = -P_2(T_1,T_2)$. This is the normal mode of heat transfer, when a hotter body cools down, and a colder one heats up. Then the left sides of equations (38) can be equated, and the corresponding quasistationary temperature of the plates is given by

$$T = \left(-\beta + \sqrt{\beta^2 + \beta(T_1^2 + T_2^2) + T_1^4 + T_2^4}\right)^{1/2}, \tag{42}$$

where $T_1$ and $T_2$ are their initial temperatures. After establishing quasithermal equilibrium, the temperature of the plates will increase according to Eqs. (40), (41).

### 3. Numerical Results

For an ideal metal without impurities and defects, within the Bloch–Grüneisen (BG) model, the damping frequency $\nu(T)$ in (6) is defined by the formula [28]

$$\nu(T) = 0.0212(\Theta/T)^5\int_0^{\Theta/T} dx x^5\sinh^{-2}(x/2)\ \text{(eV)}. \tag{43}$$

The numerical calculations were carried out using (43) and the MBG approximation shown in Figure 2 (Bloch–Grüneisen scaled). The used plasma frequency of gold is $\omega_p = 9.03$ eV. All calculations were performed with a gap width $a = 10$ nm (Figure 1) unless another value is not indicated. Note that at separations $a > 10$ nm, barely any processes of extreme heat transfer and

Preprints (www.preprints.org) | NOT PEER-REVIEWED | Posted: 13 September 2023 doi:10.20944/preprints202309.0794.v1



friction due to tunneling of electrons and phonons [32,33] and other unwanted processes do not occur [34–36].

### *3.1. Quantum Friction*

Figure 3 shows the velocity-dependent quantum friction force between the plates of gold, calculated using formulas (20) (green line), (9) (red line), and (24) (blue line).

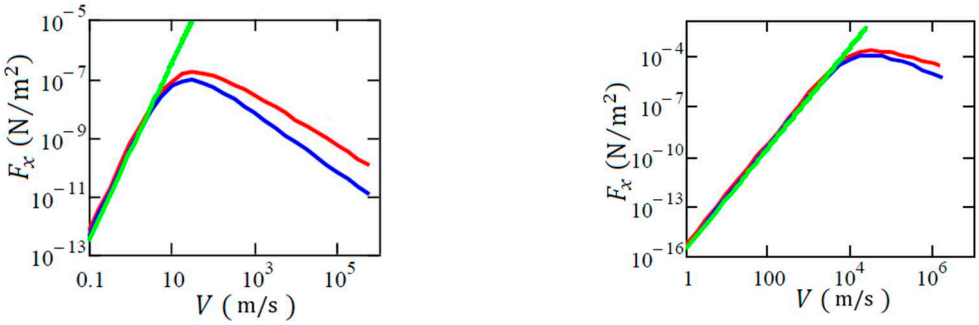


(**a**) (**b**)

**Figure 3.** Quantum friction force of the plates of gold as a function of the velocity of a moving plate 2. Panel (a): residual resistance of gold corresponds to BG model at $T = 5$ K. Panel (b): residual resistance corresponds to MBG model at $T = 0$ (Figure 2). Green, red and blue lines were calculated using Eqs. (20), (9) and (24), respectively.

The curves on panels (a) and (b) were calculated at residual resistances of $2.13 \cdot 10^{-13}$ Ω·m and $2.3 \cdot 10^{-10}$ Ω·m, which correspond to BG model (43) at $T = 5$ K and MBG model at $T = 0$ K. Note that in the latter case, the residual resistance coincides with that defined by formula (43) at $T = 20.9$ K.

### *3.2. Temperature-Dependent Friction at Thermal Quasiequlibrium*

Figure 4 shows the plots of the friction parameters $\eta = F_x/V$ depending on the temperature $T$ of gold plates, corresponding to the BG and MBG models. The curves with symbols were calculated using Eq. (9) for $V = 1$ m/s. Solid curves were plotted using approximation (25) along with (26) (green lines) or with (28) at $\lambda \gg 1$ (blue lines). On panel (a), both the solid lines merge. The presence of maxima and their positions on the curves agree with (29) and (30). These results show that the linear in velocity approximation is valid only to the right of the maxima of the dependences $\eta(T)$.

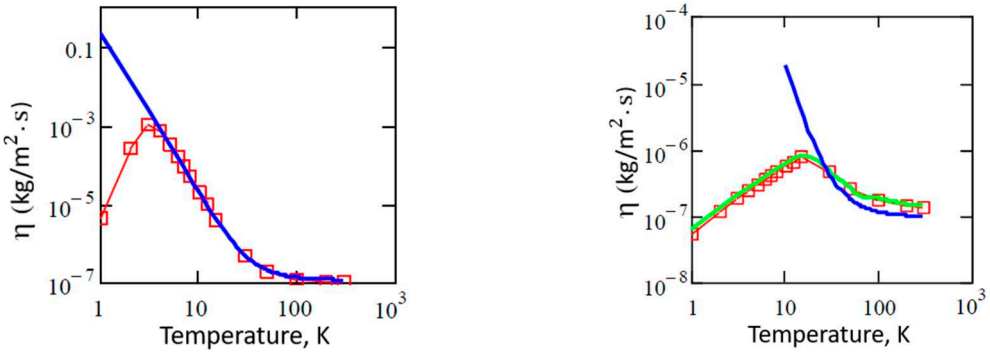


(**a**) (**b**)

**Figure 4.** Friction parameter of gold plates as a function of their quasiequilibrium temperature: (a) model BG; (b) model MBG. The curves with symbols were calculated using Eq. (9) with $V = 1$ m/s. Solid lines correspond to (25) with (26) (green lines) and (25) with (28) (blue lines in both (a) and (b)). In panel (a), both solid lines (blue and green) merge.

Preprints (www.preprints.org) | NOT PEER-REVIEWED | Posted: 13 September 2023 doi:10.20944/preprints202309.0794.v1



Figure 5 demonstrates the velocity dependences of $\eta$ in the BG model (a) and MBG model (b)). Red, blue and green lines correspond to quasiequilibrium temperatures of 5, 10, and 77 K. The different order of lines 1–3 in panels (a) and (b) is explained by the high residual resistance of gold in the MBG model: the condition $\hbar\nu(T) < T$, which is necessary for the law-temperature increase in friction, is violated at $T = 5$ and 10 K.

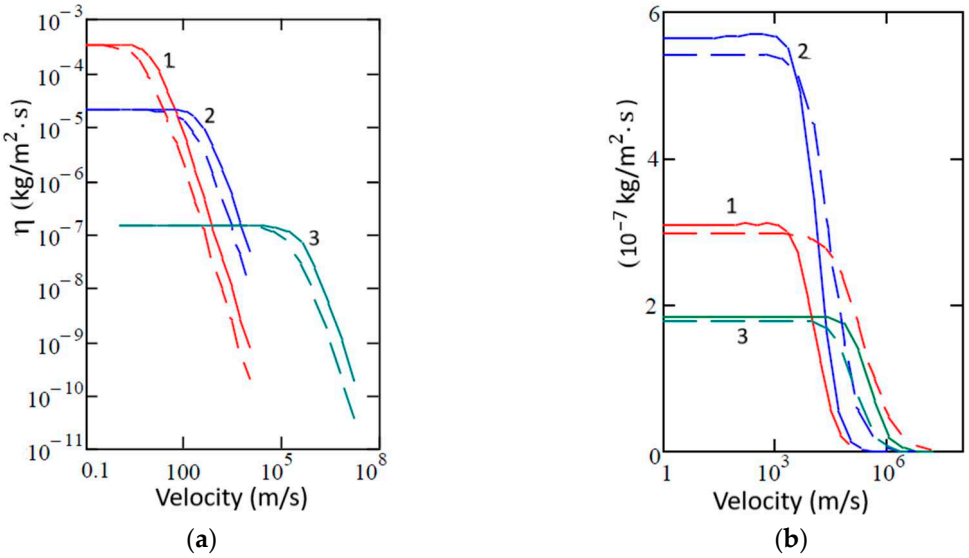


**Figure 5.** Friction parameter of gold plates as a function of the velocity of plate 2. (a) model BG; (b) model MBG. Solid lines were calculated using Eq. (9), dashed lines – Eqs. (36), (37). Red, blue and green lines 1–3 correspond to quasistationary temperatures of 5, 10, and 77 K for both plates.

Table 1 shows the calculated friction parameters $\eta$ of gold plates at $V = 1$ m/s, depending on the temperature $T$ and separation distance $a$. As in Figure 4, one can note the effect of increasing friction (up to a maximum) with decreasing temperature at $T < \theta_D$, which is more expressed in the BG model. The height of this maximum depends on the velocity-to-resistivity ratio. When the temperature becomes sufficiently low, the condition (30) is violated and the coefficient of friction decreases.

**Table 1.** Friction parameter $\eta$ (kg·m²/s) of gold plates for $V = 1$ m/s at thermal quasiequilibrium, Eq. (9)

| Temperature of plates, K | $a$ = 10 nm | $a$ = 20 nm | $a$ = 10 nm | $a$ = 20 nm |
|---|---|---|---|---|
| | Model BG | | Model MBG | |
| 1 | 4.81E-6 | 2.77E-6 | 5.60E-8 | 2.80E-8 |
| 2 | 2.63E-4 | 1.47E-4 | 1.22E-7 | 5.98E-8 |
| 3 | 1.10E-3 | 5.73E-4 | 1.87E-7 | 9.13E-8 |
| 5 | 3.44E-4 | 1.67E-4 | 3.08E-7 | 1.50E-7 |
| 10 | 2.15E-5 | 1.04E-5 | 5.63E-7 | 2.73E-7 |
| 15 | 4.30E-5 | 2.09E-6 | 7.77E-7 | 3.76E-7 |
| 20 | 1.52E-6 | 7.35E-7 | 7.19E-7 | 3.33E-7 |
| 50 | 2.04E-7 | 9.90E-8 | 2.56E-7 | 1.25E-7 |
| 100 | 1.30E-7 | 6.30E-8 | 1.77E-7 | 8.63E-8 |
| 200 | 1.14E-7 | 5.54E-8 | 1.42E-7 | 6.81E-8 |
| 300 | 1.11E-7 | 5.41E-8 | 1.39E-7 | 6.81E-8 |

The dependence of $\eta$ on the separation distance a in all the cases is close to inverse proportionality ($\eta \propto a^{-1}$). This is clearly seen from the data of the table and agrees with our previous results [19,20,27].

Preprints (www.preprints.org) | NOT PEER-REVIEWED | Posted: 13 September 2023 doi:10.20944/preprints202309.0794.v1



*3.3. Friction and Heating under Different Conditions*

Figures 6 and 7 show the calculated heating rates of plate 1 (panels (a)) and friction parameters (panels (b)) depending on the velocity $V$ of plate 2 for various thermal configurations.

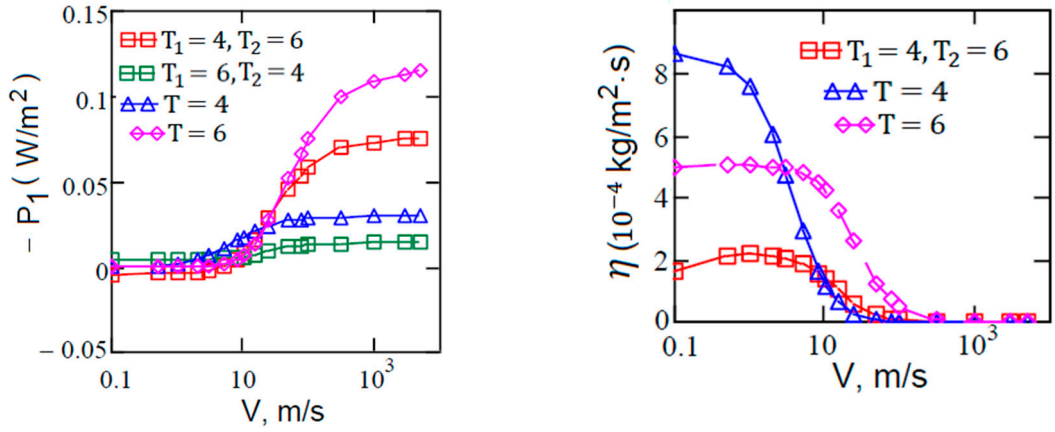


**Figure 6.** Heating rate of plate 1 (a) and friction parameter $\eta = F_x/V$ (b) in the BG model. Thermal configurations $T_1 = 6$ K, $T_2 = 4$ K and $T_1 = 4$ K, $T_2 = 6$ K have the same friction parameters, and the configurations $T = 4$ and 6 K correspond to the quasiequilibrium thermal mode. The data shown with symbols Δ (panel (a)) and ◊ (panel (b)) were increased by 3 times (see also [37]).

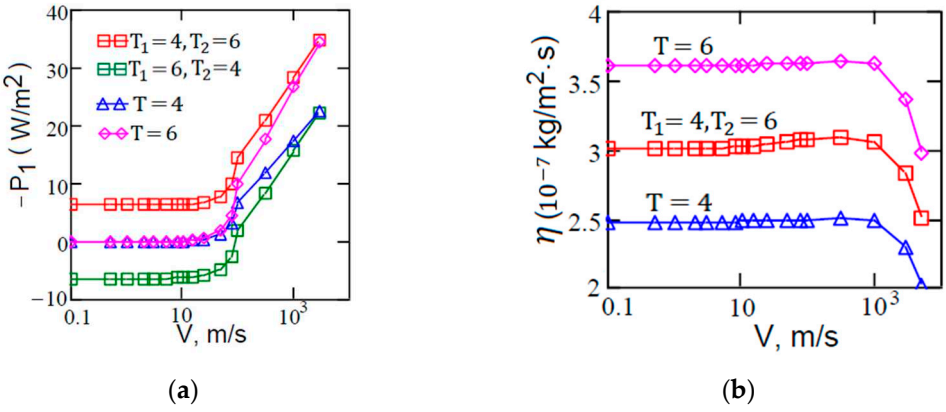


**Figure 7.** Same as in Figure 6 in the MBG model. No additional numerical factors for the data were used.

One can see that at at $V < 10$ m/s (Figure 6, panel (a)) and $V < 10^3$ m/s (Figure 7, panel (a)), the heating rates of plates 1, 2 are equal in absolute value, differing in the sign. According to their temperatures, $T_1 = 4$K and $T_2 = 6$K, plate 1 heats up and plate 2 cools down, realizing the "normal" heat exchange regime. At the same time, the friction parameters weakly depend on the temperature (panels (b)). When the speed of plate 2 becomes higher, both plates heat up faster. Then we can see the effect of "anomalous" heating of plate 2 for some time, when it continues to heat up despite the higher temperature. This is similar to the case of heating a hotter metal particle moving above a cold surface [21]. However, due to different magnitudes of the heating rate (cf. the upper and lower lines with □ on panels (a)), the temperature of plate 1 "catches up" the temperature of plate 2, and further on, both plates heat up with the same rate.

Drop in friction parameters for high velocities of plate 2 (panels (b) in Figures 6,7) is explained by the change in sign of the Doppler-shifted frequency $\omega^- = \omega - k_x V = \omega - kV\cos\phi$ in Eq. (5). This occurs at $V > v(T)a$, because the characteristic absorption frequency is $\omega \sim v(T)$ and the

Preprints (www.preprints.org) | NOT PEER-REVIEWED | Posted: 13 September 2023 doi:10.20944/preprints202309.0794.v1



characteristic wave-vector is $k \sim 1/a$. The positions of the "kinks" on the curves $\eta(V)$ in Figures 6, 7 correlate with resistivity, since $v(T) \sim \rho(T)$. Indeed, it follows from Figure 2 that $\rho_{MBG}/\rho_{BG} = 10^2 \div 10^3$ at $T = 4 \div 6$ K. At the same time, the ratio $\eta_{MBG}/\eta_{BG}$ in this case is in the inverse proportion to resistivities (see (29) and Table 1).

In general, as follows from the calculations for all considered temperatures and velocities (Figures 5–7, Table 1), the maximum friction parameter in the BG and MBG models (at $a = 10$ nm) is $10^{-6} - 10^{-3}$ kg/(m²· s).

Figure 8 shows the heating time of plates vs. velocity of plate 2, calculated by numerical integration of (39) from 4 to 5 K and from 4 to 8 K. In these calculations, the fitting parameters $a_1 = 0.0035$ J/(kg · K²), $a_2 = 0.0023$ J/(kg · K⁴) of the dependence $c(T) = a_1 T + a_2 T^3$ were determined using the data [31] for gold at $T < 20$ K.

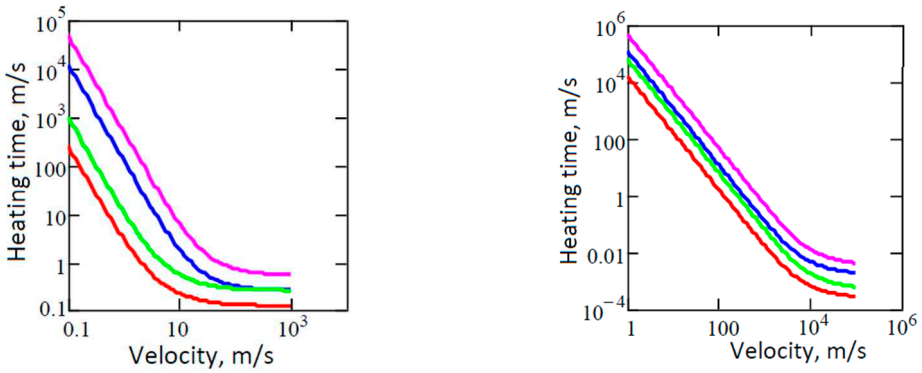


(**a**) (**b**)

**Figure 8.** Heating time of gold plates as a function of the velocity of plate 2 at $h$ = 500 μm according to BG (a) and MBG (b) models. Two upper lines correspond to heating from 4 to 8 K at $a$ = 20 nm (crimpson) and $a$ = 10 nm (blue), two lower lines correspond to heating from 4 to 5 K at $a$ = 20 nm (green) and $a$ = 10 nm (red).

As follows from Figure 8, quite comfortable (from the experimental point of view) values of the plate heating times (1–100 s) can be obtained in the velocity range 1– $10^3$m/s. On the contrary, heating by 1 K at $T_0 = 300$K, $a = 10$ nm, and $V = 10^3$ m/s will take about 2 h. Thus, low-temperature thermal measurements have great advantages over measurements under normal conditions due to a significant reduction in measurement time, elimination of noise and other undesirable effects.

## 4. Experimental Proposal

Initiated by the advantage of the experimental design [15–17] to measure the quantum friction force, in [37], I suggest to use another experimental layout shown schematically in Figure 9. Unlike paper [17], in which the setup includes a disc of 10 cm in diameter rotating with an angular frequency of up to $7 \cdot 10^3$ rps, it is proposed to use two identical discs placed in one thermostat, one of which rotates at a controlled speed. In the peripheral region, the discs have an annular metal coating with an effective area $\pi D w$. The non-inertiality of the reference system of disk 2 does not appear in this case, since the rotation frequency is small compared to the characteristic frequencies of the fluctuation electromagnetic field. Accordingly, the original expressions (2), (3) for heating rates remain valid.

Preprints (www.preprints.org) | NOT PEER-REVIEWED | Posted: 13 September 2023 doi:10.20944/preprints202309.0794.v1



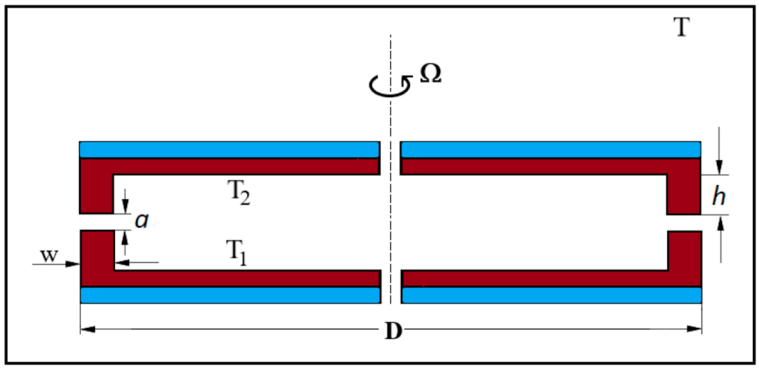


**Figure 9.** A possible setup for measuring Casimir-Lifshitz friction force (side view). The thermal protection layer is shown in blue, the metal coating is shown in red. When the upper disk rotates, the circular sections of discs locating at a distance $a$ move at a linear velocity of $0.5\Omega D$ relative to each other. At rotation frequencies $n = 1 \div 10^4$ rps and disk diameter $D = 0.1$ m, the velocity range will be 0.3÷3000 m/s.

A possible measurement scenario in this case is the quasiequilibrium thermal mode, when the temperatures of plates increase from the initial temperature $T_0$ at the same rate.

## 5. Concluding Remarks

The Casimir-Lifshitz friction force mediated by fluctuating electromagnetic field between metal plates moving with constant velocity relative to each other, causes their heating. In the state out of thermal equilibrium, "anomalous" heating of the moving plate can be observed, when it is heated for some time despite the higher temperature. However, the system rapidly reaches a state of thermal quasiequilibrium. At low temperatures $T \ll \theta_D$, the Casimir-Lifshitz friction and heating of metal plates increase significantly (see (29), (30)), while the heat capacity decreases. In combination with a fairly high speed of movement, this provides a fairly short heating time, convenient for experiments (see (40)).

**Acknowledgments:** I am grateful to Carsten Henkel for fruitful remarks at the preliminary stage of the work and for providing data on the low-temperature resistivity of gold.

**Funding:** This research received no external funding.

**Data Availability Statement:** Not applicable

**Conflicts of Interest:** The author declares no conflicts of interest.

## Appendix A. Evaluation of the Integral (24)

Substituting $t = b/2 = \zeta y \cos\phi/2$ into (22), we take into account that, typically, $\zeta y \cos\phi/2 \gg 1$ (since $\zeta \gg 1$, $y \sim 1/2\lambda \sim 1$) and $|w_{1,2}| \approx \sqrt{y^2+1}$. Then $|D|^2$ takes the form

$$|D|^2 \approx \left(y + \sqrt{y^2+1}\right)^4 \exp(-2\lambda y). \tag{A1}$$

With these simplifications, formula (18) reads

$$F_x V = -\frac{K\zeta}{2} \int_0^\infty dy \frac{y^2}{\left(y+\sqrt{y^2+1}\right)^4} e^{-2\lambda y} \int_0^{\pi/2} d\phi \frac{\cos\phi}{\psi(y,\phi)} \int_0^{\zeta y \cos\phi} dt t (\zeta y \cos\phi - t), \tag{A2}$$

$$\psi(y,\phi) = (1+\zeta^2 y^2 \cos^2\phi/4)(1+\zeta^2(1+y^2)\cos^2\phi/4) \tag{A3}$$

The $t$ integral in (A2) is simply $\zeta^3 y^3 \cos^3\phi/6$, while the integral over $\phi$ is

Preprints (www.preprints.org) | NOT PEER-REVIEWED | Posted: 13 September 2023 doi:10.20944/preprints202309.0794.v1



$$I_\phi = \frac{\zeta^3 y^3}{6}\int_0^{\pi/2} d\,\phi \frac{\cos^4\phi}{\psi(y,\phi)} = \frac{8y^3}{3\zeta}\int_0^{\pi/2} d\,\phi \frac{\cos^4\phi}{(u^2+y^2\cos^2\phi)(u^2+(1+y^2)\cos^2\phi)}, \tag{A4}$$

where $u = 2/\zeta$. The integral in (A4) is calculated explicitly using the table integral [30]

$$\int_0^{\pi/2} \frac{d\phi}{a^2+b^2\cos^2\phi} = \frac{\pi}{2}\frac{1}{a\sqrt{a^2+b^2}}. \tag{A5}$$

Using (A5) yields

$$I_\phi = \frac{4\pi y^3}{3\zeta}\left(\frac{1}{y^2(1+y^2)} - \frac{2}{y^2\sqrt{y^2\zeta^2+4}} + \frac{2}{(1+y^2)\sqrt{(1+y^2)\zeta^2+4}}\right). \tag{A6}$$

Substituting (A6) into (A2), yields (24).

**Appendix B. Evaluation of the Integral (26)**

In the case $\alpha \ll 1$, the main contribution to (26) make the values $t < 1$, $y \sim 1/2\lambda \sim 1$. Then from (14) it follows $|w_{1,2}| = |(y^2 + t/(t+i))^{1/2}| \approx y$. Using this, we find

$$|D|^{-2} \approx 16y^4\exp(-2\lambda y) \tag{B1}$$

At the same time, from (21),

$$\left(\mathrm{Im}w_{1,2}\right)^2 = \frac{t^2}{4(1+t^2)\left(y^2+t^2(1+y^2)\right)}. \tag{B2}$$

Substituting (B1) and (B2) into (26) yields

$$Y(\lambda,\alpha) = \frac{\alpha^2}{64}\int_0^\infty dyye^{-2\lambda y}\int_0^\infty dt\frac{t^2}{\sinh\,(\alpha t/2)^2}\frac{1}{(1+t^2)(y^2+t^2(1+y^2))} \tag{B3}$$

Using the approximation $\frac{t^2}{\sinh\,(\alpha t/2)^2} \to 4/\alpha^2$ and the table integral [30]

$$\int_0^\infty dx \frac{1}{(a^2+x^2)}\frac{1}{(b^2+x^2)} = \frac{\pi}{2ab(a+b)}, \tag{B4}$$

we get

$$Y_1(\lambda,\alpha) \approx \chi(\lambda) = \frac{\pi}{32}\int_0^\infty dy\frac{e^{-2\lambda y}}{\left(y+\sqrt{1+y^2}\right)} = \frac{\pi}{32}\left\{\frac{\pi}{4\lambda}[\mathrm{H}_1(2\lambda) - N_1(2\lambda)] - \frac{1}{4\lambda^2}\right\}, \tag{B5}$$

where $\mathrm{H}_1(x)$ and $N_1(x)$ are the Struve and Neumann functions [30].

**Appendix C. Evaluation of the Integral (31)**

We rewrite Eq. (13) in the form

$$Z(t,y,\phi) = \frac{2}{\exp(\alpha t)-1} - \frac{2}{\exp(\alpha|t^-|)-1}, t^- = t - \zeta y\cos\phi. \tag{C1}$$

The integral in (9) includes two exponential factors, defined by (C1). By changing the order of integration in the first term we get

$$I = 2\zeta\int_0^\infty dyy^4\int_0^\pi d\phi\cos\phi\int_0^\infty dt\frac{\mathrm{Im}w_1\mathrm{Im}w_2}{|D|^2}\frac{1}{\exp(\alpha t)-1} \tag{C2}$$

Preprints (www.preprints.org) | NOT PEER-REVIEWED | Posted: 13 September 2023 doi:10.20944/preprints202309.0794.v1



Similar to Appendix B, we can again take advantage of the behavior of the $t$- integral in (C2) for $\alpha \ll 1$, and $\zeta \gg 1$, substituting $\frac{1}{\exp(\alpha t)-1} \approx 1/\alpha t$ and using (A1) for $|D|^2$. For $\mathrm{Im}w_1\mathrm{Im}w_2$, we use (21) with the replacement $|t-b| \to \zeta y|cos\phi|$. Then (21) takes the form

$$\mathrm{Im}w_1\mathrm{Im}w_2 = -\frac{t\cdot\zeta|\cos\phi|\cdot \mathrm{sign}(t-\zeta y cos\phi)}{4\left[(1+\zeta^2y^2\cos^2\phi)(1+\zeta^2(1+y^2)\cos^2\phi)(1+t^2)\left(y^2+t^2(1+y^2)\right)\right]^{1/2}}. \quad \text{(C3)}$$

Inserting (C3) into (C2) yields

$$I = \frac{\zeta^2}{\alpha}\int_0^\infty dy \frac{y^4e^{-2\lambda y}}{\left(y+\sqrt{y^2+1}\right)^4(1+y^2)^{1/2}}\int_0^{\pi/2} d\phi\psi_1(y,\phi)\int_0^\infty dt\,\psi_2(t,y), \quad \text{(C4)}$$

where

$$\psi_1(\phi,y) = \cos^2\phi[(1+\zeta^2y^2\cos^2\phi)(1+\zeta^2(1+y^2)\cos^2\phi)]^{-1/2}, \quad \text{(C5)}$$

$$\psi_2(t,y) = \frac{1}{\left[(1+t^2)\left(\frac{y^2}{(1+y^2)}+t^2\right)\right]^{1/2}}. \quad \text{(C6)}$$

Substituting (C5) and (C6) into (C4) and taking into account (B4), the inner integrals are calculated yielding (see (35) and three lines upper)

$$I_\phi(y) = \int_0^\infty d\phi\frac{\cos^2\phi}{\psi_1(\phi,y)} \approx \frac{\pi}{2\zeta^2}\left[\frac{\sqrt{1+\zeta^2y^2}-1}{y^2\sqrt{1+\zeta^2y^2}} + \frac{\sqrt{1+\zeta^2(1+y^2)}-1}{(1+y^2)\sqrt{1+\zeta^2(1+y^2)}}\right], \quad \text{(C7)}$$

$$I_t(y) = \int_0^\infty dt\,\psi_2(t,y) = \frac{1}{\sqrt{1+y^2}}\mathrm{K}\left(\frac{1}{\sqrt{1+y^2}}\right), \quad \text{(C8)}$$

where $\mathrm{K}(x)$ is the elliptic integral. Finally, substituting (C7) and ((C8) into (C4) yields

$$I = \frac{\pi}{4\alpha}\int_0^\infty dy\frac{y^4e^{-2\lambda y}}{\left(y+\sqrt{y^2+1}\right)^4(1+y^2)^{1/2}}\mathrm{K}\left(\frac{1}{\sqrt{1+y^2}}\right)\left[\frac{\sqrt{1+\zeta^2y^2}-1}{y^2\sqrt{1+\zeta^2y^2}} + \frac{\sqrt{1+\zeta^2(1+y^2)}-1}{(1+y^2)\sqrt{1+\zeta^2(1+y^2)}}\right]. \quad \text{(C9)}$$

The second integral in (9) including $t^-$ in (C1) is evaluated with the same result (but ultimately having the opposite sign), by introducing a new variable $t' = t-b$, and using the substitution $|t'+b| \to \zeta y|\cos\phi|$ in (21).

## References


1. Casimir, H.B.G. On the attraction between two perfectly conducting plates. *Proc. Kon. Ned. Akad. Wet. B* **1948**, *51*, 793–795.
2. Lifshitz, E.M. The theory of molecular attractive forces between solids. *Sov. Phys. JETP* **1956**, *2*, 73–83.
3. Yablonovitch, E. Accelerating reference frame for electromagnetic waves in a rapidly growing plasma: Unruh-Davies-Fulling-DeWitt radiation and the nonadiabatic Casimir effect. *Phys. Rev. Lett.* **1956**, *62*, 1742–1746. https://doi.org/10.1103/PhysRevLett.62.1742
4. Dodonov, V.V.; Klimov, A.B.; and Man'ko ,V.I. Nonstationary Casimir effect and oscillator energy level shift. *Phys. Rev. Lett. A*, **1989**, 142, 511-513. https://doi.org/10.1016/0375-9601(89)90525-2
5. Schwinger, J. Casimir energy for dielectrics. *Proc. Nat. Acad. Sci. USA* **1989**, *89*, 4091–4093. https://doi.org/10.1073/pnas.89.9.4091
6. Dodonov, V. Fifty years of the dynamic Casimir effect. *Physics* **2020,** *2*, 67-104
7. Mostepanenko, V.M. Casimir puzzle and Casimir conundrum: discovery and search for resolution. *Universe* **2021**, *7*, 704084. https://doi.org/10.3390/universe7040084

8. Reiche, D.; Intravaia, F.; Busch, K. Wading through the void: exploring quantum friction and vacuum fluctuations. APL Photonics **2022**, 7, 030902. https://doi.org/10.1063/5.0083067
9. Volokitin, A.I.; Persson, B.N.J. Near-field radiation heat transfer and noncontact friction. Rev. Mod. Phys. **2007**, *79*, 1291–83. https://doi.org/10.1103/RevModPhys.79.1291
10. Milton, K.A.; Høye, J.S.; Brevik, I. The reality of Casimir friction. *Symmetry* **2016**, *8*, 29–83.
11. Pendry, J.B. Shearing the vacuum –quantum friction. *J. Phys. C.: Condens. Matter* **1997**, *9*, 10301–10320.
12. Stipe, B.C.; Stowe, T.D.; Kenny, T.W.; Rugar, D. Noncontact friction and force fluctuations between closely spaced bodies. *Phys. Rev. Lett.* **2001**, *87*(9), 096801.
13. Volokitin, A.I. Casimir friction force between a $SiO_2$ probe and a graphene-coated $SiO_2$ substrate. *JETP Lett.* **2016**, *104*, 534-539. https://doi.org/10.1134/S0021364016190139
14. Volokitin, A.I. *JETP Lett.* Effect of an electric field in the heat transfer between metals in the extreme near field. **2019**, *110*, 749–754. https://doi.org/10.1134/S002136401911016X
15. Viotti, L.; Farias, M.B.; Villar, P.I.; Lombardo, F.C. Thermal corrections to quantum friction and decoherence: A closed time-path approach to atom-surface interaction. *Phys. Rev. D*, **2019**, *99*, 105005. https://doi.org/10.1103/PhysRevD.99.105005
16. Farias, M.B.; Lombardo, F.C.; Soba, A.A.; Villar, P.I.; and Decca, R.S. Towards detecting traces of non-contact quantum friction in the corrections of the accumulated geometric phase. *npj Quantum Inf.* **2020**, *6*, 25. https://doi.org/10.1038/s41534-020-0252-
17. Lombardo, F.C.; Decca, R.S.; Viotti, L., and Villar, P.I. Detectable signature of quantum friction on a sliding particle in vacuum. *Adv. Quant. Tech.* **2021**, *4*, 2000155.
18. Gurudev Dutt, M.V.; Childress, L.; Jiang, L.;Togan, E.; Maze, J.; Jelezko, F.; Zibrov, A.S.; Hemmer, P.R.; , and Lukin, D. Quantum register based on individual electronic and nuclear spin qubits in diamond. *Science* (Washington, DC, U.S.), **2007**, *316(5829)*,1312. DOI: 10.1126/science.1139831
19. Dedkov, G.V. Low-temperature increase in the van der Waals friction force with the relative motion of metal plates. *JETP Lett.* **2021**, *114*, 779–784. https://doi.org/10.31857/S1234567821230105
20. Dedkov, G.V. Puzzling low-temperature behavior of the van der Waals friction force between metallic plates in relative motion. *Universe* **2021**, *7*, 427. https://doi.org/10.3390/universe7110427
21. Dedkov, G.V. Nonequilibrium Casimir-Lifshitz friction force and anomalous radiation heating of a small particle. *Appl. Phys. Lett.* **2022**, *121*, 231603.
22. Guo, X.; Milton, K.A.; Kennedy, G.; McNulty, W.P.; Pourtolami, N.; and Li, Y. Energetics of quantum friction: Field fluctuations [arXiv:2108.01539], *Phys. Rev. D* **2021**, *104*, 116006**.**
23. Guo, X.; Milton, K.A.; Kennedy; G., McNulty, W.P.; Pourtolami, N.; and Li, Y. Energetics of quantum friction. II: Dipole fluctuations and field fluctuations. [arXiv:2204.10886], *Phys. Rev. D* **2022**, *106*, 016008.
24. Milton, K.A.; Guo, X.; Kennedy, G.; Pourtolami, N.; and DelCol., D.M. Vacuum torque, propulsive forces, and anomalous tangential forces: Effects of nonreciprocal media out of thermal equilibrium. [arXiv:2306.02197], https://doi.org/10.48550/arXiv.2306.02197
25. Reiche, D.; F. Intravaia, F.; Hsiang, J.-T.; Busch, K.; and Hu, B.-L. Nonequilibrium thermodynamics of quantum friction. *Phys. Rev.* **2020**, *102*, 050203(R).
26. Polevoi, V.G. Tangential molecular forces between moving bodies by a fluctuating electromagnetic field. *Sov. Phys. JETP* **1990**, *71*, 1119–1124.
27. Dedkov, G.V.; Kyasov, A.A. Friction and radiative heat exchange in a system of two parallel plate moving sideways: Levin-Polevoy-Rytov theory revisited. *Chin. Phys.* **2018**, *56*, 3002. https://doi.org/10.1016/j.cjph.2018.10.006.
28. *Handbook of Physics*, 1967, 2nd ed. E.U. Condon and H. Odishaw (New York: McGraw-Hill) equation (6.12).
29. Baptiste, J. in: *The Physics Factbook*, Ed. by Elert, G. (2004). https://hypertextbook.com/facts/2004/JennelleBaptiste.shtml
30. Gradshteyn, I. S. and Ryzhik, I.M., Table of Integrals, Series and Products, 8th ed. (Academic Press, Waltham, MA, 2014).
31. *Handbook of Physical Quantities*, Ed. By Grigoriev, I.S.; Meilikhov, E.Z. (Energoatomizdat, Moscow, 1991; CRC Boca Raton, NY, 1996).
32. Biehs, S.-A.; Kittel, A.; Ben-Abdallah, P. *Z. Naturforsch.* **2020**, *75*,802.
33. Viloria, M.G.; Guo, Y.; Merabia, S.; Ben-Abdallah, P.; Messina, R. Role of Nottingham effect in the heat transfer in extreme near field regime. *Phys. Rev.* **2023**, *107*, 125414. https://doi.org/10.1103/PhysRevB.107.125414

34. Pendry, J.B., Sasihithlu K.; Kraster R.V. Phonon-assisted heat transfer between vacuum-separated surfaces. *Phys. Rev. B* **2016**, *94*,075414. https://doi.org/10.1103/PhysRevB.94.075414
35. Sasihithlu, K.; Pendry, J.B. Van der Waals force assisted heat transfer. *Z. Naturforsch.* **2017**, *72*, 181. https://doi.org/10.1515/zna-2016-0361
36. Kuehn S.; Loring R.F.; Marohn, J.A. Dielectric fluctuations and the origins of noncontact friction. *Phys. Rev.* **2006**, *96*, 156103. https://doi.org/10.1103/PhysRevLett.96.156103
37. Dedkov, G.V. Casimir-Lifshitz friction force and kinetics of radiative heat transfer between metal plates in relative motion. *JETP Lett.* **2023**, *117*, 952 [It is worth noting that all numerical data in this paper must be reduced by $\pi$ times].